Dielectric function of $LaAlO_3$ from 0.8 to 6 eV between 77 and 700 K

Cayla Marie Nelson, Maria Spies, Lina S. Abdallah, and Stefan ZollnerYun Xu and Hongmei Luo

Citation: J. Vac. Sci. Technol. A **30**, 061404 (2012); doi: 10.1116/1.4754811
View online: http://dx.doi.org/10.1116/1.4754811
View Table of Contents: http://avs.scitation.org/toc/jva/30/6
Published by the American Vacuum Society

Dielectric function of $LaAlO_3$ from 0.8 to 6 eV between 77 and 700 K

Cayla Marie Nelson, Maria Spies, Lina S. Abdallah, and Stefan Zollner[a)]
Department of Physics, New Mexico State University, MSC 3D, P.O. Box 30001, Las Cruces, New Mexico 88003-8001

Yun Xu and Hongmei Luo
Department of Chemical Engineering, New Mexico State University, MSC 3805, P.O. Box 30001, Las Cruces, New Mexico 88003-3805

(Received 2 August 2012; accepted 12 September 2012; published 4 October 2012)

The authors used spectroscopic ellipsometry to determine the dielectric function and the refractive index of $LaAlO_3$ as a function of photon energy from 0.8 to 6 eV between 77 and 700 K. The ellipsometric angles were acquired over a broad range of incidence angles with a computer-controlled Berek waveplate compensator and with zone-averaging of the adjustable polarizer. The data were corrected for surface effects, such as surface roughness or adsorbed overlayers. The authors report Tauc–Lorentz model parameters for $LaAlO_3$ at 300 K. After annealing in UHV for 20 h, the surface layer thickness decreased from 15 Å to less than 1 Å. They speculate that the anneal causes surface modifications, such as the evaporation of adsorbed molecular layers (hydrocarbons or water) or surface vacancies, and that surface diffusion leads to a reduction of surface roughness. They have also measured the temperature-dependence of the refractive index at 1.96 eV between 77 and 700 K and given a theoretical explanation of its origin. © *2012 American Vacuum Society*. [http://dx.doi.org/10.1116/1.4754811]

I. INTRODUCTION

Lanthanum aluminate ($LaAlO_3$ or LAO) is a polar perovskite oxide that is used widely as a substrate material for oxide epitaxy.[1] It can be viewed as an alternating stack of positively charged LaO and negatively charged AlO_2 planes. It has created much attention because a two-dimensional electron gas can be formed in $LaAlO_3/SrTiO_3$ heterostructures.[2]

Despite the high level of interest in LAO, our knowledge of its optical properties is limited.[3–8] Gibbons and Trolier-McKinstry[3] used spectroscopic ellipsometry (with a compensator for increased accuracy) from 250 to 750 nm at a fixed angle of incidence to determine the real part of the dielectric function ϵ of LAO as a function of wavelength λ. They also modeled their data with a Sellmeier oscillator

$$\epsilon(\lambda) = 1 + \frac{A\lambda^2}{\lambda^2 - \lambda_0^2} \tag{1}$$

and determined the Sellmeier parameters $A = 3.08 \pm 0.01$ and $\lambda_0 = 125.5 \pm 2.2$ nm. Lim *et al.*[4] performed transmission measurements on an LAO substrate and found the onset of weak absorption at 5.5 eV. They also measured the dielectric function from 5 to 9 eV using a vacuum-ultraviolet (VUV) rotating-analyzer spectroscopic ellipsometer (without compensator) and found two strong peaks in e_2 between 7 and 8 eV. They presented a model of the band structure where the valence band is made up of oxygen 2p states and the conduction band is formed by the antibonding 5d and 6s states of lanthanum. The weaker absorption from 5.5 to 7 eV is caused by interband transitions from the O (2p) to La (5d) states. The stronger absorption above 7 eV arises from transitions from O (2p) to La (6s) or, possibly,[9] to antibonding Al (sp) states. *Ab initio* calculations of the dielectric function (without considering corrections to the local density functional band structure or many-body effects) show a more complex conduction band structure that also includes transitions to the La (4f) conduction band.[10,11]

Finally, Cicerella *et al.*[5] investigated a 300 nm thick film of amorphous LAO on Si using VUV ellipsometry. They found the onset of absorption at 6.3 eV (consistent with transmission measurements by Motorola[6]) and reported the absorption coefficient up to 9 eV but not the refractive index (or ϵ_1) for their films. Edon *et al.* show that sputtered $LaAlO_3$ films on Si have a somewhat lower ϵ_1 than bulk samples, which drops even lower after annealing in oxygen.[7]

II. EXPERIMENT AND MODELS

A single-side polished, 2-in. $LaAlO_3$ wafer with 0.5 mm thickness and (100) surface orientation was obtained commercially.[12] The manufacturer specified a surface roughness below 8 Å. $LaAlO_3$ is a distorted perovskite with rhombohedral ($R\bar{3}c$) crystal structure,[13] but the deviations from the cubic structure are small.[1] Our substrate is twinned and the surface orientation refers to the pseudo-cubic structure. Our wafer was colorless and smooth as-received, perhaps with a very slight tan color. After annealing at 700 K in UHV for several hours, the samples darkened slightly and formed macroscopic surface streaks. It has been reported[13] that LAO turns brown after annealing at 710 K for 5 min. The color is associated with oxygen vacancies[13] or color centers. At 813 K, LAO becomes cubic with $Pm\bar{3}m$ crystal structure.[13] We do not know if our as-received polished surface is LaO or AlO_2-terminated.

a)Electronic mail:zollner@nmsu.edu

We acquired the ellipsometric angles ψ and Δ on a vertical variable-angle-of-incidence rotating-analyzer ellipsometer with a computer-controlled Berek waveplate compensator.[14] We usually chose incidence angles between 60° and 80°. The detector and optics are suitable for measurements from 0.5 to 6.6 eV, but the choice of the optical fiber between the monochromator and the polarizer-sample-analyzer assembly limits spectra to the IR range (0.5–4.5 eV) or the UV range (0.76–6.6 eV). The low refractive index of $LaAlO_3$ reduces the intensity of the reflected beam and thus limits the spectral range in the UV portion of the spectrum under certain conditions. To reduce experimental errors, especially in the presence of windows, all data were obtained by averaging two-zone measurements with equal and opposite polarizer angles.

The ellipsometric angles (ψ and Δ) and the Fresnel reflectance ratio $\rho = e^{i\Delta} \tan \psi$ are related to the pseudo-refractive index $\hat{n}$ and the pseudo-dielectric function $\hat{\epsilon} = \hat{n}^2$ of the sample through[15,16]

$$\rho = \frac{(\hat{n}\cos\phi_0 - \cos\phi_1)(\cos\phi_0 + \hat{n}\cos\phi_1)}{(\hat{n}\cos\phi_0 + \cos\phi_1)(\cos\phi_0 - \hat{n}\cos\phi_1)}, \tag{2}$$

where ϕ_0 is the angle of incidence and ϕ_1 the angle of refraction. For an ideal sample without surface overlayers, $\hat{n}$ and $\hat{\epsilon}$ are equal to the refractive index n and the dielectric function $\epsilon = n^2$. Δ equals zero or π for an ideal transparent substrate, because all quantities in Eq. (2) are real.

In practice, surface effects including surface roughness, adsorbed molecular films, surface modifications (such as oxygen vacancies at the surface to avoid the polar catastrophe[1] caused by the polar character of LAO), or native oxides (in the case of semiconductors or metals) can cause a pseudo-absorption (with arbitrary values of Δ), even for a transparent overlayer on a transparent substrate.[17] The influence of surface roughness on the ellipsometry spectra is normally described using the Bruggeman effective medium approximation, assuming a surface layer consisting of 50% bulk and 50% voids.[15] Since ellipsometry is unable to distinguish between the various types of surface effects, we describe all surface effects as surface roughness and ignore other effects. This is reasonably accurate, as long as surface layers are thin and have a refractive index lower than that of the bulk.

We not only acquired data in air, but also mounted the sample in a UHV cryostat[18] that allowed cooling of the sample to 77 K using liquid nitrogen and resistive heating of the sample to 700 K. A base pressure below 10^{-8} Torr could be achieved with the sample at 300 K after several days of pumping. The entrance and exit fused-silica windows of the cryostat are additional optical (polarizing) elements in the beam path.[19] The ellipsometric angles ψ_W and Δ_w of these windows were carefully calibrated as a function of photon energy using an oxidized silicon reference sample at a 70° angle of incidence. Since the angle between the optical beam and the window surfaces is small ($\sim 3°$), Δ_w is a much more significant correction than ψ_W. All our spectra taken in the cryostat were corrected for window artifacts by the manufacturer's data acquisition software.[20] The temperature was measured using an extended type-E thermocouple located a few inches from the sample in the copper cryogen reservoir near the resistive heating element. The sample was clamped to the copper coldfinger using spring-loaded screws or with a UHV-compatible silver nanoparticle adhesive. The coldfinger is connected to the copper reservoir with screws and a thin metal gasket. We confirmed proper performance of the cooling and heating functions of the cryostat by determining the E_1 and $E_1 + \Delta_1$ critical-point parameters of Ge as a function of temperature, resulting in parameters similar to those of Viña *et al.*[21,22]

The complex dielectric function ϵ for a material can often be described by a simple oscillator model, such as the Sellmeier equation (1). We note that the Sellmeier equation predicts only dispersion and not absorption. This is not Kramers–Kronig consistent but is a workable approximation for materials well below the onset of absorption. For our work, we prefer a Tauc–Lorentz oscillator, where the imaginary part of ϵ as a function of photon energy E is given by[16,23,24]

$$\epsilon_2(E) = \frac{AE_0\Gamma(E - E_g)^2}{E[(E^2 - E_0^2)^2 + \Gamma^2 E^2]}, \tag{3}$$

for $E > E_g$ and vanishes below E_g. The real part is obtained by Kramers–Kronig transform. This model works well for amorphous materials and can be a good approximation for crystalline materials, if the absorption can be described by a single broad peak. The model contains the following parameters: E_g is the Tauc gap, the onset of absorption. Based on the value of the band gap established in Ref. 4, we fix $E_g = 5.6$ eV. The remaining three parameters were fitted to our data: the Lorentz oscillator resonance energy E_0, its amplitude A, and its broadening Γ. Additionally, we use a pole

$$\epsilon(E) = \frac{A_1}{E_1^2 - E^2} \tag{4}$$

at energy $E_1 = 0.01$ eV with magnitude $A_1 = 0.018\ \text{eV}^2$ (determined by fitting) to describe the infrared lattice absorption. (A pole is a Lorentz oscillator with zero broadening.[15])

III. RESULTS: MEASUREMENTS AT 300 K

First, we measured the ellipsometric angles of one quarter of our wafer as received, without any cleaning, at four angles of incidence (60°, 65°, 70°, 75°). An excellent fit (where the mean square deviation between data and model is smaller than the measurement errors) could be achieved with a roughness layer thickness of 21 Å and the Tauc–Lorentz parameters given in Table I. Next, we degreased the wafer through ultrasonic cleaning in acetone, followed by a methanol rinse and drying in nitrogen. This decreased the surface roughness to 18 Å, see Table I. Degreasing a different quarter of the same wafer on slightly different equipment resulted in a surface roughness thickness of 15 Å. The depolarization of the reflected light in our measurements is less than 0.01% at $\phi_0 = 65°$ and becomes slightly negative ($\sim -0.3\%$) at $\phi_0 = 80°$ indicating small systematic errors.

TABLE I. Summary of room-temperature measurements of $LaAlO_3$ in air with Tauc–Lorentz parameters. These parameters listed here describe our experimental results. They may not be unique and therefore no error bars are given.

Sample	Angles	Roughness(Å)	A	E_0(eV)	Γ(eV)
As received	60°–75°	21	243.7	9.025	3.989
Degreased	55°–80°	18	252.3	8.946	4.407
Degreased	70°	15	253.3	8.942	4.449
After removal	60°–80°	32	206.8	9.278	2.169

The ellipsometric angles for the degreased wafer are shown in Fig. 1 at several angles of incidence. Because of the low refractive index of $LaAlO_3$ ($\hat{n} \sim 2.06$ at 2 eV, which corresponds to a pseudo-Brewster angle of 64°), ψ is usually very small except for angles of incidence greater than 70°. Larger incidence angles thus increase the accuracy of the refractive index measurement. Δ is near 0 for large incidence angles and near π for smaller angles, requiring the use of a compensator to achieve accurate results. Deviations from 0 or π are related to the surface roughness thickness.[17] Where the incidence angle equals the pseudo-Brewster angle $(\tan\hat{\phi}_B = \hat{n})$, Δ crosses from 0 to π. Since the refractive index of $LaAlO_3$ increases with increasing photon energy (positive dispersion), the cross-over shifts to higher energies with increasing incidence angles. The width of this cross-over is determined by the surface roughness. At $\phi_0 = 70°$, ψ decreases from 10° to 3° and Δ increases from 1° to 45° as the photon energy increases from 0.76 to 6.6 eV. At the wavelength of the HeNe laser ($E = 1.96$ eV), $\psi = 9.6°$ and $\Delta = 2.4°$ for $\phi_0 = 70°$.

After acquiring data in air, the $LaAlO_3$ wafer was mounted in a UHV cryostat with ellipsometry windows, but we did not turn on the pumps. The purpose of this measurement was to test the effect of the windows on the ellipsometry measurements and check the window calibration. The measurement of the sample in the cryostat (but at atmospheric pressure, in air) gives the same values for ψ as in air, but below the band gap (5.5 eV) Δ is much lower than in air, see Fig. 2. Above the band gap, Δ is about the same in air and in the cryostat.

After turning on the vacuum pumps and pumping down to 10^{-5} Torr, the measurement was repeated and the ellipsometric angles did not change (not shown). Next, we heated the sample at 700 K in UHV for 1 h and allowed the sample to cool down overnight. Again, the ellipsometric angles did not change (not shown). Finally, we heated the sample at 700 K for 20 h in UHV and allowed it to cool down overnight. Again, there is little change in Δ but a very significant drop of Δ below the band gap. At 1.96 eV, Δ has dropped to 0.4°, consistent with 3 Å roughness thickness, much lower than the roughness specified by the manufacturer. (8 Å rms roughness measured by atomic force microscopy should result in an ellipsometric roughness layer thickness of 15–20 Å.) A Tauc–Lorentz model with roughness does not yield a satisfactory description of the ellipsometric angles inside the cryostat (before or after cooling). Such low values of Δ are unexpected. Therefore, the experiment was repeated with a different quarter cleaved from the same $LaAlO_3$ wafer. For the second sample, the value of Δ found at 1.96 eV was even lower (0.1°), corresponding to a roughness layer thickness of 0.5 Å. The depolarization of the reflected light did not

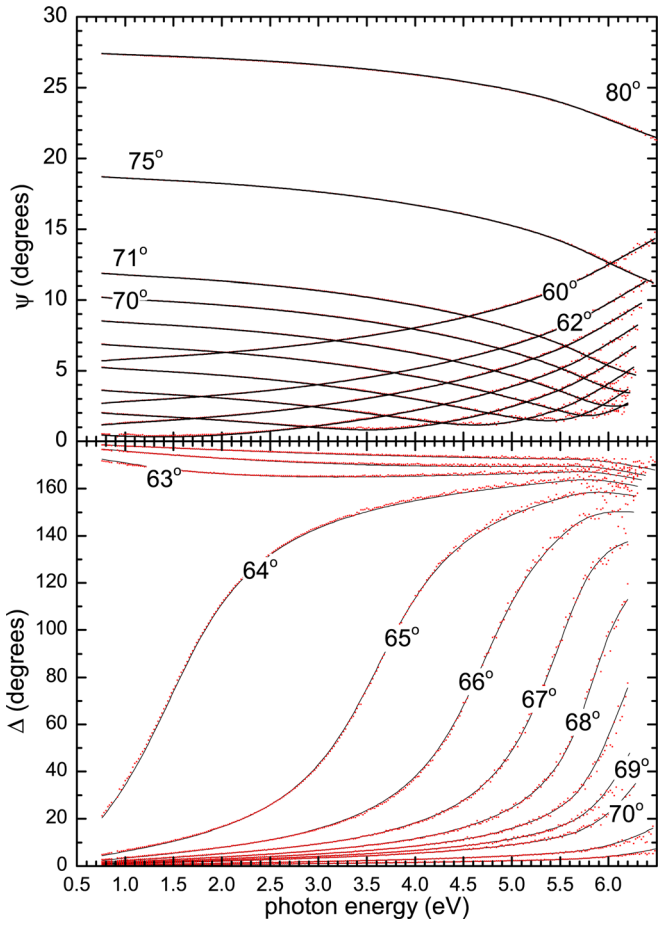

FIG. 1. (Color online) Symbols: Ellipsometric angles ψ and Δ for a $LaAlO_3$ substrate measured in air (after degreasing) at various angles of incidence (60°, 62°, 63°, 64°, 65°, 66°, 67°, 68°, 69°, 70°, 71°, 75°, 80°). Lines: Calculated data based on a Tauc–Lorentz model for the substrate with 18.5 Å surface roughness.

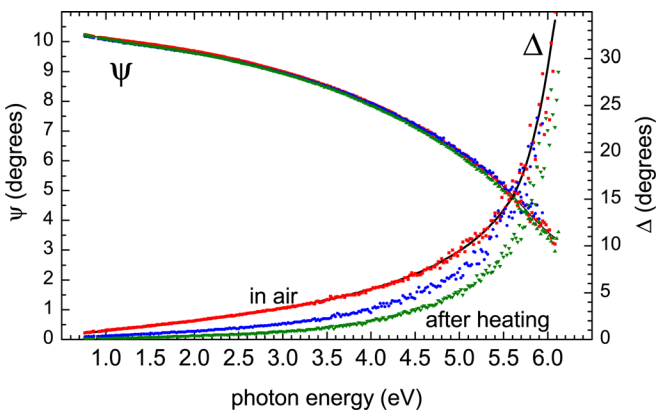

FIG. 2. (Color online) Symbols: Ellipsometric angles for degreased $LaAlO_3$ at 70° angle of incidence in air (■), in cryostat at atmospheric pressure in air (◆), at 10^{-8} Torr after UHV anneal at 700 K for 20 h (▼). Lines: Tauc–Lorentz fit to the data in air, see Table I.

increase when mounting the wafer in the cryostat or annealing the sample.

After annealing the $LaAlO_3$ sample in UHV and several measurements, the sample was removed from the cryostat and measured again in air. The surface layer thickness for this sample had increased quite significantly, to 32 Å, as shown in Table I.

IV. DISCUSSION OF 300 K RESULTS

We summarize our results as follows: The ellipsometry spectra of $LaAlO_3$ from 0.76 to 6 eV are described very well with a Tauc–Lorentz layer for the substrate with a thin surface roughness layer, see Table I. Between 250 and 750 nm (1.65–5 eV), our results are in good agreement with the Sellmeier parameters found in Ref. 3, but the dispersion becomes stronger at higher photon energies closer to and above the band gap, see Fig. 3.

Below the band gap, the values of Δ are much lower inside the cryostat (at atmospheric pressure in air, under UHV conditions, or after a UHV anneal) than for measurements in air outside the cryostat. Above the band gap (5.5 eV), the values of Δ are about the same for all our measurements. This result cannot be explained by window effects, which increase linearly with photon energy. We also find that the reduction in Δ persists with small changes of the incident angle (between 68° and 72°), which should modulate the systematic errors due to windows.

The decrease in Δ below the band gap (at a constant refractive index) must be associated with a reduction of the surface layer thickness. We offer the following possible explanations: (1) Adsorbed molecular surface films (water or hydrocarbons) evaporate in UHV, especially after annealing at 700 K. (2) After adsorbed surface layers are removed, the LAO surface is modified, for example, by formation of lanthanum or oxygen vacancies, to avoid the polar catastrophe.[1,25,26] (3) The formation of surface vacancies is associated with significant atomic displacements.[1,26] We speculate that there is significant surface diffusion under a UHV anneal at 700 K. Therefore, the polishing-induced roughness of the as-received surface (with small correlation lengths) is replaced by larger, flat terraces and macroscopic streaks. In the ellipsometry spectra, this surface change is seen as a decreased surface layer thickness. These proposed explanations could be confirmed by scanning probe microscopy under UHV conditions before and after annealing.

As mentioned, a Tauc–Lorentz oscillator model for $LaAlO_3$ with surface overlayer effects does not give a satisfactory description of the ellipsometry spectra. This can also be seen in Fig. 3: The absorption vanishes (or is close to zero) below 3 eV, indicating a very small surface layer thickness below 1 Å. On the other hand, $\hat{\epsilon}_2$ is significant between 4 eV and the bulk bandgap of 5.5 eV. We speculate that the surface modifications associated with the desorption of surface overlayers cause electronic surface states, which are the reason for the absorption below the band gap.

V. TEMPERATURE-DEPENDENT MEASUREMENTS (80–700 K)

We also cooled the $LaAlO_3$ sample to 77 K by filling the cryostat with liquid nitrogen. The comparison between the data taken just before the cooldown (at 300 K) and just after the cooldown (at 77 K) is shown by the pseudodielectric functions in Fig. 4. There is no measurable difference in $\hat{\epsilon}$. We conclude that the temperature dependence of ϵ for $LaAlO_3$ between 77 and 300 K is very small. The measurement at 77 K was repeated after keeping the sample cold for several hours. This third measurement (blue) shows a slight increase in $\hat{\epsilon}_2$, indicating growth of a surface layer caused by the condensation of residual gas in the cryostat on the cold sample surface. Keeping the sample cold even longer grew a thicker surface layer, as indicated by an additional measurement at 77 K a few hours later (not shown). (Similar measurements of the temperature-dependence of the $LaAlO_3$ dielectric function were performed by Stewart *et* al.,[27] but we do not believe that these results have been published.) From our spectroscopic scans shown in Fig. 4, we find $\epsilon_1 = 4.25 \pm 0.01$ (or $n = 2.06 \pm 0.01$) at 1.96 eV independent of temperature, which limits $|dn/dT| < 4 \times 10^{-5} K^{-1}$.

Since the (relative) precision of ellipsometry measurements is greater than the (absolute) accuracy, we also present measurements of the pseudodielectric function $\hat{\epsilon}$ at a fixed photon

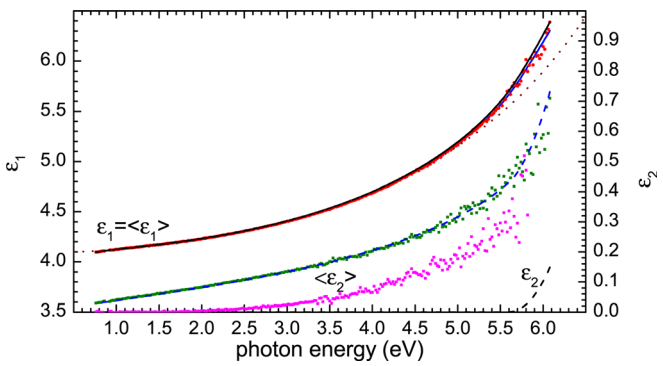

FIG. 3. (Color online) Symbols: Pseudo-dielectric function for degreased $LaAlO_3$ in air (red: $\hat{\epsilon}_1$, green: $\hat{\epsilon}_2$) and in UHV after annealing at 700 K (magenta: $\hat{\epsilon}_2$). Blue lines: Fit to experimental data in air with Tauc–Lorentz layer and surface roughness. Black lines: Optical constants ($\hat{\epsilon}_1, \hat{\epsilon}_2$) for $LaAlO_3$ calculated from the Tauc–Lorentz parameters for the sample in air. Dotted line: Sellmeier dispersion given by Eq. (1).

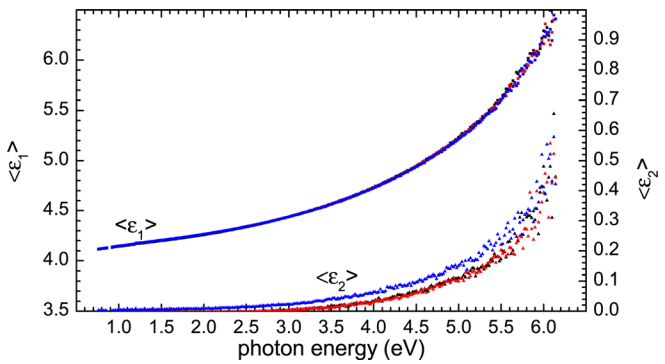

FIG. 4. (Color online) Real and imaginary parts of the pseudodielectric function of $LaAlO_3$ measured at 300 K in the cryostat (black), at 77 K (red), and again at 77 K several hours later (blue). A measurement at 700 K also yields similar results.

energy of 1.96 eV, taken between 80 K and 700 K with a ramp rate of 1 K/min, see Fig. 5. Over the entire temperature range, $\hat{\epsilon}$ is essentially zero within our measurement errors. The real part $\hat{\epsilon}_1$ initially decreases from 4.246 at 80 K to 4.242 at 250 K. At higher temperatures, there is an almost linear increase of $\hat{\epsilon}_1$ between 250 and 700 K. The slope of this graph yields $d\epsilon/dT = 2 \times 10^{-5}/\mathrm{K}$ or $dn/dT = 5 \times 10^{-6}/\mathrm{K}$.

A simple theory for the high-frequency dielectric constant ϵ_∞ (far above the energy of lattice absorption, but well below the onset of electronic absorption), similar to the long-wavelength limit of the pole in Eq. (4), states that[28]

$$\epsilon_\infty = 1 + (E_p/E_{\mathrm{Penn}})^2, \tag{5}$$

where E_{Penn} is the average separation of the conduction and valence bands, also known as the Penn gap, and E_p the plasma energy of the valence electrons given by

$$E_p^2 = \frac{\hbar^2 N e^2}{m\epsilon_0}, \tag{6}$$

where $2\pi\hbar$ is Planck's constant, N the density of valence electrons per unit volume, e the electronic charge, m the effective electron mass, and ϵ_0 the permeability of vacuum. A photon energy of 1.96 eV satisfies the requirements of being between the vibrational and electronic absorption regimes and this equation should apply. The Penn gap is often similar to the E_2 gap in many semiconductors.[28] Based on the VUV ellipsometry results in Ref. 4 and our Tauc–Lorentz models (see Table I), we speculate that $E_{\mathrm{Penn}} \sim 8$ eV. The temperature dependence of ϵ_∞ therefore has two components: (1) The thermal expansion of the crystal, which decreases N and therefore is negative. (2) The temperature dependence of the Penn gap, which should be positive if the Penn gap decreases with increasing temperature.

It follows from Eq. (5) that the temperature dependence of ϵ_∞ due to thermal expansion is given by

$$\left(\frac{d\epsilon_\infty}{dT}\right)_{\mathrm{expansion}} = (\epsilon_\infty - 1)\frac{d\ln N}{dT} = -\beta(\epsilon_\infty - 1), \tag{7}$$

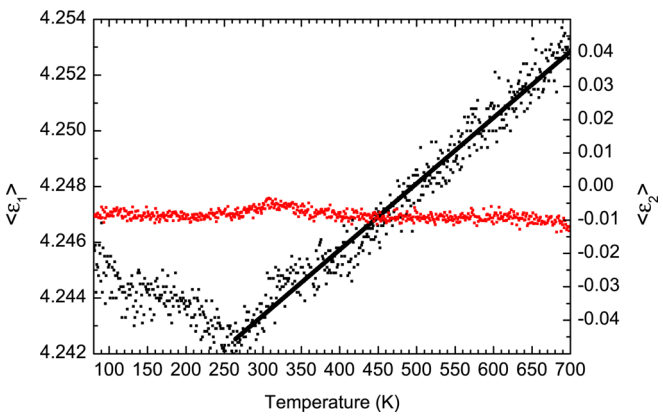

FIG. 5. (Color online): Real (black) and imaginary (red) parts of the pseudo-dielectric function of $LaAlO_3$ vs temperature at a fixed photon energy of 1.96 eV. The straight line shows a linear fit to the $\hat{\epsilon}_1$ data between 250 and 500 K.

where β is the volume expansion coefficient. This contribution is negative. Using a value of $\beta = 3 \times 10^{-5}/\mathrm{K}$ for LAO (Ref. 13) between 250 and 700 K, we find the thermal expansion contribution to the temperature dependence of ϵ_∞ to be $-10^{-4}/\mathrm{K}$. This term is five times larger than the experimentally observed value ($2 \times 10^{-5}/\mathrm{K}$) and it has the wrong sign.

We, therefore, conclude that the temperature dependence of the Penn gap is the dominant term leading to the increase of ϵ_∞ between 250 and 700 K. From Eq. (5), it follows that

$$\left(\frac{d\epsilon_\infty}{dT}\right)_{\mathrm{Penn}} = -2(\epsilon_\infty - 1)\frac{d\ln E_{\mathrm{Penn}}}{dT}. \tag{8}$$

A negative dE_{Penn}/dT produces an increase of ϵ_∞ with temperature. Let us assume that the Penn gap decreases with temperature at a rate of -2.5×10^{-4} eV/K, similar to the E_2 gap of Si.[29] This yields $d\epsilon_\infty/dT = 2 \times 10^{-4}/\mathrm{K}$.

Our theoretical analysis of the temperature dependence of ϵ_∞ between 250 and 700 K therefore finds that there are two contributions (from the Penn gap and the thermal expansion of the crystal), which are of the same order of magnitude ($10^{-4}/\mathrm{K}$), but opposite in sign. These two contributions cancel mostly, resulting in a measured value of $d\epsilon_\infty/dT$, which is an order of magnitude smaller than each of the two individual contributions.

In the low-temperature regime between 80 and 250 K, both the thermal expansion coefficient and the temperature dependence of the Penn gap are much smaller than at higher temperatures.[13,29] Both follow a Varshni-type relationship,[30] where a quadratic dependence on temperature dominates at low temperatures. Based on our result that $d\epsilon_\infty/dT$ is negative below room temperature, we conclude that the thermal expansion term dominates in this regime.

The temperature dependence of n was also investigated in the Terahertz regime by Zou *et al.*[31] They found that dn/dT is small (not specified) and related to oxygen vacancies and lattice vibrations. In contrast, dn/dT in the visible range reported in this work is related to electronic excitations, see Eq. (5).

VI. CONCLUSIONS

We used spectroscopic ellipsometry to investigate the optical properties (complex dielectric function and refractive index) of bulk $LaAlO_3$. We report Tauc–Lorentz parameters that can be used for a parametric description of the dielectric function of $LaAlO_3$ in air. We also found that the thickness of the $LaAlO_3$ surface layer (adsorbed molecular layers or surface roughness) decreases significantly after annealing in UHV at 700 K for many hours. We speculate that the UHV anneal desorbs molecular atmospheric contamination and reduces the surface roughness by surface diffusion and formation of very large terraces. The temperature-dependence of the high-frequency dielectric constant is small but can be understood in terms of thermal expansion and the decrease of the Penn gap with increasing temperature. Both terms are similar in magnitude but have opposite signs. The thermal expansion contribution dominates below room temperature,

while the temperature dependence of the Penn gap dominates at room temperature and above.

ACKNOWLEDGMENTS

This work was supported by the National Science Foundation (DMR-1104934) and by the New Mexico State University Vice President for Research (IRG 118422, URIG 120163). The authors are grateful to Eric DeLong for technical assistance.

[1]H. Seo and A. A. Demkov, Phys. Rev. B **84**, 045440 (2011).
[2]A. Ohtomo and H. Y. Hwang, Nature (London) **427**, 423 (2004).
[3]B. J. Gibbons and S. Trolier-McKinstry, IEEE Trans. Appl. Supercon. **7**, 2177 (1997). The Sellmeier equation in this reference contains a misprint, which we have corrected in Eq. (1).
[4]S.-G. Lim *et al.*, J. Appl. Phys. **91**, 4500 (2002).
[5]E. Cicerella, J. L. Freeouf, L. F. Edge, D. G. Schlom, T. Heeg, J. Schubert, and S. A. Chambers, J. Vac. Sci. Technol. A **23**, 1676 (2005).
[6]X.-B Lu, Z.-G. Liu, Y.-P. Wang, Y. Yang, X.-P. Wang, H.-W. Zhou, and B.-Y. Nguyen, J. Appl. Phys. **94**, 1229 (2003).
[7]V. Edon, M. Gaillet, M. C. Hugon, C. Eypert, O. Durand, and C. Cardinaud, Phys. Status Solidi C **5**, 1206 (2008).
[8]A. Marino, A. Rubano, D. Paparo, L. Marrucci, U. Scotti di Uccio, F. Miletto Granozio, C. Aruta, M. Fiebig, and J. Mannhart, 7th Workshop Ellipsometry, Leipzig, Germany, 5–7 March 2012 (unpublished).
[9]P. W. Peacock and J. Robertson, J. Appl. Phys. **92**, 4712 (2002).
[10]X. Luo and B. Wang, J. Appl. Phys. **104**, 053503 (2008).
[11]G. Murtaza and I. Ahmad, J. Appl. Phys. **111**, 123116 (2012).
[12]See www.mtixtl.com for MTI Corporation, Richmond, CA.
[13]S. A. Hayward *et al.*, Phys. Rev. B **72**, 054110 (2005).
[14]J. A. Woollam Co., Inc., Lincoln, NE, Model V-VASE.
[15]H. G. Tompkins and W. A. McGahan, *Spectroscopic Ellipsometry and Reflectometry* (Wiley, New York, 1999).
[16]H. Fujiwara, *Spectroscopic Ellipsometry* (Wiley, Chichester, UK, 2007).
[17]G. E. Jellison and B. C. Sales, Appl. Opt. **30**, 4310 (1991).
[18]J. A. Woollam Co., Inc., Lincoln, NE, Model CRV-727V. See User's Manual for a description of window calibration.
[19]R. M. A. Azzam and N. M. Bashara, J. Opt. Soc. Am. **61**, 773 (1971).
[20]B. D. Johs and C. M. Herzinger, U.S. patent 6,034,777 (7 March 2000).
[21]L. Viña, S. Logothetidis, and M. Cardona, Phys. Rev. B **30**, 1979 (1984).
[22]A. A. Medina, L. S. Abdallah, and S. Zollner, *AVS 59th International Symposium*, Tampa, FL, 28 October–2 November 2012.
[23]G. E. Jellison, in *Handbook of Ellipsometry*, edited by H. G. Tompkins and E. A. Irene (Springer, Heidelberg, 2005), p. 237.
[24]G. E. Jellison and F. A. Modine, Appl. Phys. Lett. **69**, 371 (1996); **69**, 2137 (1996).
[25]X. Luo, B. Wang, and Y. Zheng, Phys. Rev. B **80**, 104115 (2009).
[26]J.-L. Tang, J. Zhu, W.-F. Qin, J. Xiong, and Y.-R. Li, Chinese Phys. B **17**, 655 (2008).
[27]M. K. Stewart, J. Liu, M. Kareev, J. Chakhalian, and D. N. Basov, Phys. Rev. Lett. **107**, 176401 (2011). See also supplemental materials for this article.
[28]P. Yu and M. Cardona, *Fundamentals of Semiconductors* (Springer, Berlin, 1996), p. 325.
[29]P. Lautenschlager, M. Garriga, L. Vina, and M. Cardona, Phys. Rev. B **36**, 4821 (1987).
[30]Y. P. Varshni, Physica (Utrecht) **34**, 149 (1967).
[31]X. Zou *et al.*, AIP Adv. **2**, 012120 (2012).